FABRICATION AND CHARACTERIZATION OF NANO-Fe/WOODCERAMIC COMPOSITES

*Wei Hong Zhou**†*

Lecturer
E-mail: zhouweihong2005@163.com

Yun Shui Yu

Professor
College of Material Science and Engineering
Central South University of Forestry and Technology
Changsha 410004, People's Republic of China
E-mail: yuyunshui@sina.com

Xue Liang Xiong

Professor
Institute of Mineral Resources Development and Utilization
Changsha Research Institute of Mining and Metallurgy Limited Company
Changsha 410004, People's Republic of China
E-mail: xiong9550@163.com

(Received September 2017)

Abstract. Furan resin added with γ-Fe_2O_3 nanoparticles and Chinese fir sawdust were mixed and compressed into boards. The boards were then sintered in a vacuum furnace to obtain a nano-Fe/woodceramic composite. The phase constitution, microstructure, and element distribution of the composite were examined by using X-ray diffraction (XRD), scanning electron microscopy (SEM), and energy disperse spectroscopy (EDS), respectively. The mechanical properties, volume electrical resistivity, and wave adsorption properties were investigated. XRD analysis indicates that α-Fe, Fe_3C, and graphite carbon exist in the nano-Fe/woodceramic composite, and α-Fe promotes the graphite degree of woodceramic. SEM and EDS observations indicate that the composite has a porous structure and α-Fe nanoparticles distributed in the woodceramic. Experimental results show that the maximum values of bending strength and compressive strength are 11.74 MPa and 13.86 MPa, respectively. The minimum value of volume electrical resistivity is 0.021 Ω·cm. The minimum reflection loss value is −11.45 dB at 9.68 GHz with 3 mm thickness of absorbing layer.

Keywords: Nano-Fe, woodceramic, γ-Fe_2O_3 nanoparticles, mechanical properties, microwave adsorption properties.

INTRODUCTION

A porous carbon material obtained by carbonizing woody material impregnated with thermosetting resin in a vacuum furnace is called a woodceramic (Okabe et al 1996). The woody material changes into soft amorphous carbon, and the thermosetting resin changes into hard glassy carbon reinforcing the soft carbon. According to reports, there are mainly two technical routes to fabricate woodceramics. The first technical route is as follows: the solid wood or medium-density fiberboard is impregnated with thermosetting resin and then carbonized at a temperature of 300-2800°C in a vacuum furnace (Kano et al 1997; Li et al 2002). The second technical route is as follows: first, sawdust or other biomass particles are mixed with a thermosetting resin or liquefied wood; then, the mixture is molded into boards; and last, the boards are carbonized in a vacuum furnace (Hirose et al 2001; Hirose et al 2002; Yu et al 2012). Raw materials of woodceramics are a wide range of sources, including wood, bamboo,

* Corresponding author
† SWST member

Wood and Fiber Science, 50(4), 2018, pp. 381-391
https://doi.org/10.22382/wfs-2018-050

bagasse, straw, and other renewable resources (Zhao et al 2002; Li and Li 2006; Wu 2008; Xing et al 2010).Therefore, woodceramic is an environment-friendly material. Some research on the mechanical properties, friction properties, electromagnetic (EM) shielding properties, morphologies, and damping properties of woodceramic have been performed (Shibata et al 1997; Akagaki et al 1999; Qian et al 2004; Zhang et al 2005).

Recently, microwave absorption materials have attracted much attention for their properties of eliminating or reducing the EM interference pollution and radar detection for military defense purposes. The performances of microwave absorption materials depend on their dielectric and magnetic losses. There have been some reports on carbon materials as dielectric loss materials including carbon black, carbon nanotubes (single-walled carbon nanotubes and mutiwalled carbon nanotubes), and graphite (Oh et al 2004; Liu et al 2007; Xu et al 2013). Woodceramic is a carbon material primarily composed of amorphous carbon and glassy carbon. In addition, the porous structure of woodceramics can improve the multireflection of EM waves. Therefore, woodceramic has potential applications in the fields of microwave adsorption. However, there have been no reports on woodceramics as a microwave absorber so far.

Nanoparticles have specific EM properties. Ferromagnetic metal nanoparticles (Fe, Co, Ni, and their alloys) have strong interaction with high frequency EM waves because of their great permeabilities. In this study, we propose to fabricate a nano-Fe/woodceramic composite, which could improve the microwave absorption and mechanical properties of woodceramic. Furfural phenol resin has a high carbon yield ratio and the furfural is originated from agriculture byproducts such as wheat bran, corn cob, and so on. Therefore, in this study, furan resin was used as the impregnating resin instead of phenolic resin commonly used by other researchers. Fe nanoparticles have high chemical activities and are apt to be oxidized severely, even combust in the air. Therefore, γ-Fe_2O_3 nanoparticles are used as raw material to obtain Fe nanoparticles through carbothermal reduction reaction. Furthermore, the effects of addition content of γ-Fe_2O_3 nanoparticles on the mechanical properties, volume electrical resistivity, and wave adsorption properties of nano-Fe/woodceramic composites are investigated in detail.

MATERIALS AND METHODS

Material Preparation

Chinese fir (*Cunninghamia lanceolata*) was smashed by using a grinder into sawdust with a mean particle size of 420 μm with a moisture content of 6%. Furan resin was synthetized in the laboratory. The synthetic process was as follows: furfural was mixed with phenol with the mass ratio of 3:4, and then they sufficiently reacted at 135°C for 4 h, using K_2CO_3 as catalyst. γ-Fe_2O_3 nanoparticles (20 nm, 99.5% purity, purchased from Shanghai Aladdin Bio-Chem Technology Co., Ltd., Shanghai, China) aggregated when they were taken out of the reagent bottle. Therefore, they were first grinded using a mortar and pestle in ethanol medium for 30 min to form a uniform suspension and then poured into furan resin with different mass contents of 3%, 7%, 10%, 15%, and 25%. The furan resin added with γ-Fe_2O_3 nanoparticles was then mixed thoroughly with the Chinese fir sawdust. In addition, a mixture that only included furan resin and Chinese fir sawdust was prepared for comparison. Samples with their raw material composition were shown in Table 1. These mixtures were dried at 60°C for 10 h, and then pressed under a pressure of 50 MPa for 25 min at 170°C to obtain boards, the dimensions of which were about 100 mm × 50 mm × 25 mm.

Table 1. Samples with their raw material composition.

Samples	Mass of raw material of WCM (%)		Addition content of γ-Fe_2O_3 to resin (%)
	Chinese fir sawdust	Furan resin	
WCM	60	40	0
WCM-3	60	40	3
WCM-7	60	40	7
WCM-10	60	40	10
WCM-15	60	40	15
WCM-25	60	40	25

Last, these boards were sintered in a vacuum furnace to form nano-Fe/woodceramic composites. The maximum sintering temperature was 800°C (Shibata et al 1997; Hirose et al 1999). The temperature of the furnace was raised at a heating rate of 3°C/min to 800°C, keeping for 1 h at 400°C and keeping for 3 h at 800°C in the heating process.

Characterization

The microstructure of the nano-Fe/woodceramic composites was examined by using a scanning electron microscope (SEM; Helios Nanolab 600i; FEI Company, Hillsboro, OR) operated at 10 kV. The distribution of Fe was examined by energy disperse spectroscopy (EDS; X-Max^N; Oxford Instruments, Oxford, UK).

The phase of the nano-Fe/woodceramic composites was examined by using a X-ray diffractometer (XRD; XD-2; Beijing Purkinje General Instrument Co., Ltd., Beijing, China) with Cu-K_α radiation at a scanning rate of $8^\circ \cdot \text{min}^{-1}$ over an angle range of 10-90° (2θ).

The bending strength of nano-Fe/woodceramic composites was tested by using a universal mechanical testing machine (MWD-50; Jinan Testing Machine Factory, Jinan, China). The crosshead speed was 2 $\text{mm} \cdot \text{min}^{-1}$. The dimensions of the samples were about 80 mm × 12 mm × 4 mm. Five samples were tested to obtain an average value.

The compressive strength of nano-Fe/woodceramic composites was tested by using a universal mechanical testing machine (WDW-10; Jinan Xinshijin Testing Machine Co., Ltd., Jinan, China). The crosshead speed was 5 $\text{mm} \cdot \text{min}^{-1}$. The dimensions of the samples were about 20 mm × 10 mm × 4 mm. Five samples were tested to obtain an average value.

The volume electrical resistivity of the nano-Fe/woodceramic composite was recorded by using a four-probe meter (RTS-8; Guangzhou Four-Point Probe Technology Co., Ltd., Guangzhou, China). Five measurements were performed to obtain an average value for every sample.

The EM parameters, including complex permittivity ($\varepsilon = \varepsilon' - j\varepsilon''$) and complex permeability ($\mu = \mu' - \mu''$), were measured by using a vector network analyzer (8720ET; Agilent Technologies Inc., Santa Clara, CA) in the frequency range of 2-18 GHz which both civil and military applications widely used. The test samples were prepared as follows: first, crush and grind the nano-Fe/woodceramic composite into a powder with a grain size of about 74 μm; then, mix this powder and melted wax homogeneously in a mass ratio of 1:2; and last, place the mixture in the steel molds and press to concentric ring samples. The outer diameter was 7 mm, the inner diameter was 3.04 mm, and the thickness was about 3 mm. The mold of the concentric ring is shown in Fig 1. Based on the resultant EM parameters, the reflection loss (RL) could be calculated according to Eqs 1 and 2.

$$\text{RL} = 20 \log \left| \frac{Z_{\text{in}} - 1}{Z_{\text{in}} + 1} \right|, \tag{1}$$

$$Z_{\text{in}} = \sqrt{\frac{\mu}{\varepsilon}} \tanh\left(j \frac{2\pi}{\lambda} d \sqrt{\varepsilon \times \mu} \right), \tag{2}$$

where Z_{in} is the normalized input impedance of the absorber, μ is the complex permeability, ε is the complex permittivity, λ is the wavelength, and d is the thickness of the absorber.

Figure 1. Mold of concentric ring.

RESULTS AND DISCUSSION

XRD Analysis

Figure 2 shows the XRD patterns of the nano-Fe/woodceramic composites and woodceramics for comparison. The pattern of woodceramics shows two broad peaks corresponding to (002) peak at 24° (2θ) and (101) peak at 44° (2θ) of graphite crystal, which indicates that the Chinese fir sawdust and furan resin have changed into carbon material with a graphite-like structure. The (002) peak is asymmetric and broad, which indicates a disordered stack of graphene sheets and tiny graphite crystals in the woodceramic. It can be found from Fig 2 that the intensity of these peaks, corresponding 2θ of which is 45°, 65°, and 82°, become stronger and stronger as the addition content of γ-Fe_2O_3 nanoparticles increases. Referring to the Powder Diffraction File, 44.6732° (2θ), 65.0211° (2θ), and 82.3326° (2θ) are the right 2θ angles corresponding to (110), (200), and (211) diffraction peaks of α-Fe, respectively. Consequently, the existence of α-Fe in the composite is confirmed. It is obvious from the intensity of these peaks that the amount of α-Fe increases with the increasing of addition content of γ-Fe_2O_3 nanoparticles. The other diffraction peaks at around 2θ = 37.8°, 42.9°, 46.0°, 48.7°, and 49.1° are attributed to the (210), (211), (112), (131), and (221) planes of Fe_3C, which indicates that a small amount of Fe_3C exists in the composite.

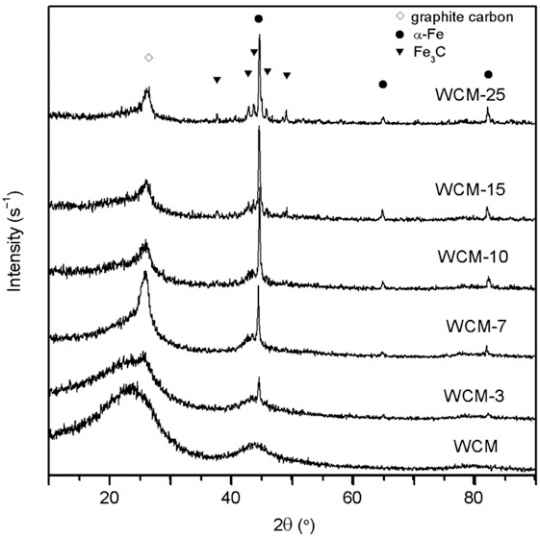

Figure 2. X-ray diffraction patterns of the nano-Fe/woodceramic composites with different weight percentages of γ-Fe_2O_3 nanoparticles.

α-Fe is in-situ produced from γ-Fe_2O_3 by carbothermal reduction reaction. Furthermore, a small amount of α-Fe reacts with carbon to form Fe_3C. With the increasing of addition content of γ-Fe_2O_3 nanoparticles, the (002) peak of woodceramic gets narrow and sharp, which means that the graphite microcrystallites in woodceramic grow. This result indicates that iron particles have the catalytic graphitization effect on woodceramics. The small size of α-Fe particles enable them to diffuse through the woodceramic matrix at the relatively low temperature and a graphitic phase precipitates after dissolution and precipitation of carbon atoms from the iron particles (Marsh et al 1983).

SEM Analysis

Figure 3a shows the microstructure of WCM-7. It can be seen that the composite inherits the porous structure of wood. Figure 3b shows the plane scanning distribution of Fe of Fig 3a, and Table 2 shows the chemical composition of the plane scanning area. It can be seen from Fig 3b that element Fe is well distributed in woodceramic. Table 2 shows that carbon has the highest weight and atomic percentage, oxygen has the second highest weight and atomic percentage, and iron has the third highest weight and atomic percentage. Carbon and oxygen originate from the organic components of Chinese fir sawdust and furan resin. Iron originates from γ-Fe_2O_3 nanoparticles. There exists a minor amount of potassium, calcium, silicon, and sulfur. All of the elements originate from the ash of Chinese fir sawdust.

Figure 4 shows the backscattered electron images of the nano-Fe/woodceramic composites. It can be seen from Fig 4 that there are lots of α-Fe nanoparticles dispersed in the woodceramic. The addition content of γ-Fe_2O_3 nanoparticles has an

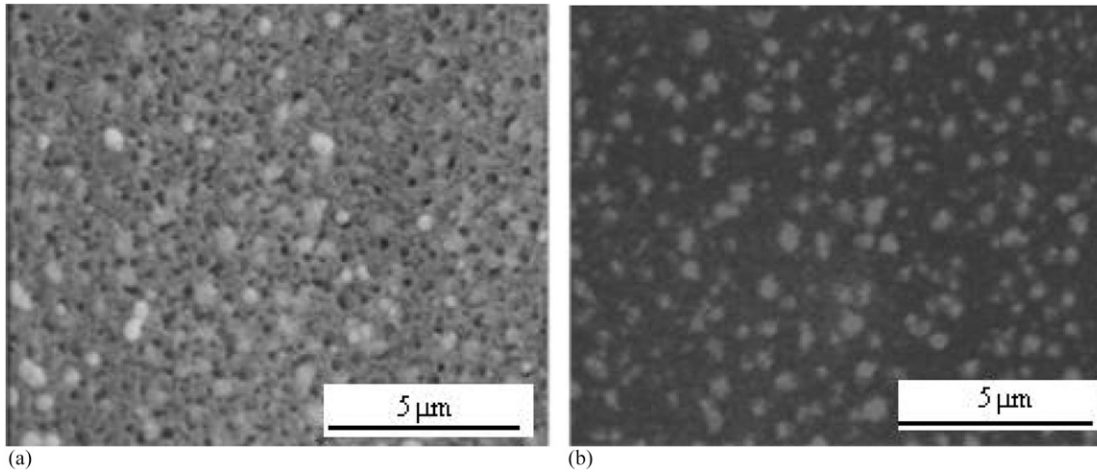

(a) (b)

Figure 3. (a) Microstructure of WCM-7 (b) plane scanning distribution of Fe of (a).

important effect on the particle size of α-Fe. Most α-Fe particle sizes are less than 100 nm as the addition content is no more than 7%. However, with the increasing of addition content of γ-Fe_2O_3 nanoparticles, α-Fe particles grow up significantly and local agglomeration takes place. This phenomenon may be mainly caused by the volume shrinkage of woodceramics in the sintering process. Some particle sizes are more than 100 nm as shown in Fig 4c-e.

Mechanical Properties

Figure 5 shows the influence of addition content of γ-Fe_2O_3 nanoparticles on the mechanical strength of the nano-Fe/woodceramic composites. With the increasing of addition content of γ-Fe_2O_3 nanoparticles, the bending strength of the nano-Fe/woodceramic composites first increases and then decreases. The maximum value of the bending strength, 11.74 MPa, is obtained when the addition content of γ-Fe_2O_3 nanoparticles is 15%, increasing by 35.25% compared with that of the woodceramic. The influence of the addition content of γ-Fe_2O_3 nanoparticles on the compressive strength of the nano-Fe/woodceramic composites is also shown in Fig 5. It is shown that the compressive strength of the nano-Fe/woodceramic composites first increases and then decreases with the increasing of the addition content of γ-Fe_2O_3 nanoparticles. The maximum value of the compressive strength, 13.86 MPa, is obtained when the addition content of γ-Fe_2O_3 nanoparticles is 15%, increasing by 57.32% compared with that of the woodceramic.

Table 2. Chemical composition of the plane scanning area.

Element	Weight (%)	Atomic (%)
C	81.85	0.90
O	8.80	0.07
Si	0.06	0.00
S	0.06	0.00
K	1.41	0.00
Ca	0.07	0.00
Fe	7.74	0.02

One reason for this phenomenon is the improvement of graphitization degree of woodceramics, and the other is the strengthening effect of α-Fe nanoparticles on woodceramics. Figure 6 shows the SEM photograph of the fracture surface of WCM-15. The fracture surface shows two different surface characteristics. One part shows a smooth surface where no α-Fe nanoparticles disperse, and the other part shows a rough surface where some small cracks could be found where a lot of α-Fe nanoparticles disperse. A big crack can be seen in throughout the fracture surface. One part of the big crack in the smooth fracture surface shows a straight and smooth

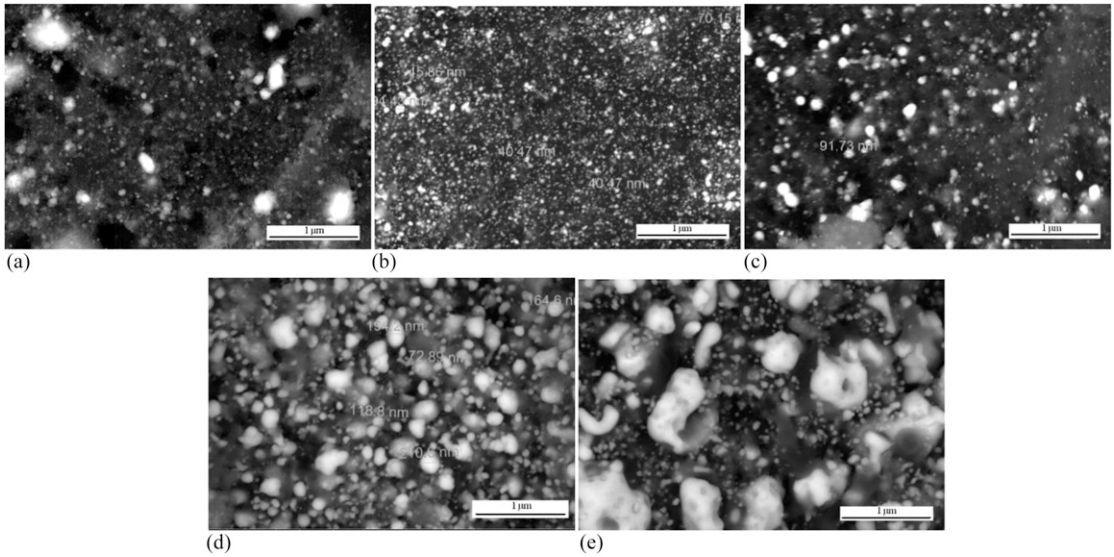

Figure 4. Backscattered electron images of the nano-Fe/woodceramic composites (×100,000) (a) WCM-3 (b) WCM-7 (c) WCM-10 (d) WCM-15 (e) WCM-25.

surface. On the contrary, the other part of the big crack in the rough fracture surface shows a zigzag, which indicates that α-Fe nanoparticles can hinder the expanding of the crack tip under stress. According to the wall-bending model (Lizuka et al 1999), the cracks are initiated at the wall consisting of a wood layer and resin layer. α-Fe nanoparticles disperse in the wall. Therefore, the wall is strengthened.

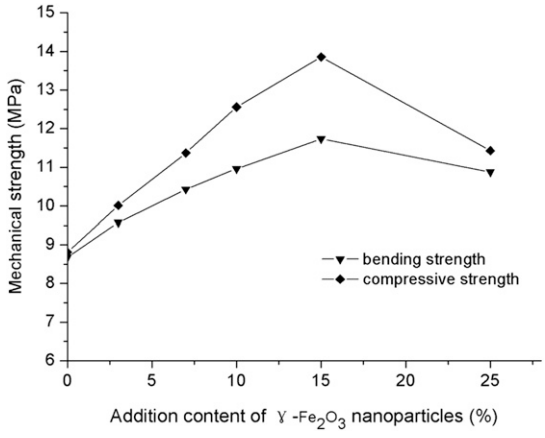

Figure 5. Influence of addition content of γ-Fe_2O_3 nanoparticles on the mechanical strength of the nano-Fe/woodceramic composites.

However, the bending strength and compressive strength decrease when addition content of γ-Fe_2O_3 nanoparticles increases to 25%, for visible big cracks appear in the nano-Fe/woodceramic composites that may be induced by the difference of thermal expansion coefficient between α-Fe aggregates (>100 nm) and the woodceramic.

Volume Resistivity

Figure 7 shows influence of addition content of γ-Fe_2O_3 nanoparticles on the volume electrical resistivity of the nano-Fe/woodceramic composites. As shown in Fig 7, the volume electrical resistivitiy of the nano-Fe/woodceramic composites reduces as the addition content of γ-Fe_2O_3 nanoparticles increases. As the addition content of γ-Fe_2O_3 nanoparticles increases from 0 to 25%, the volume electrical resistivity reduces from 0.039 Ω·cm to 0.021 Ω·cm, decreasing by 46%. In woodceramic, there exist two kinds of carbon with different microstructure including turbostratic carbon and graphite carbon. Graphite carbon has better electrical conductivity than that of turbostratic carbon. α-Fe can accelerate the ordered stacking of graphene sheets and growth of graphite microcrystalline. As a consequence, the

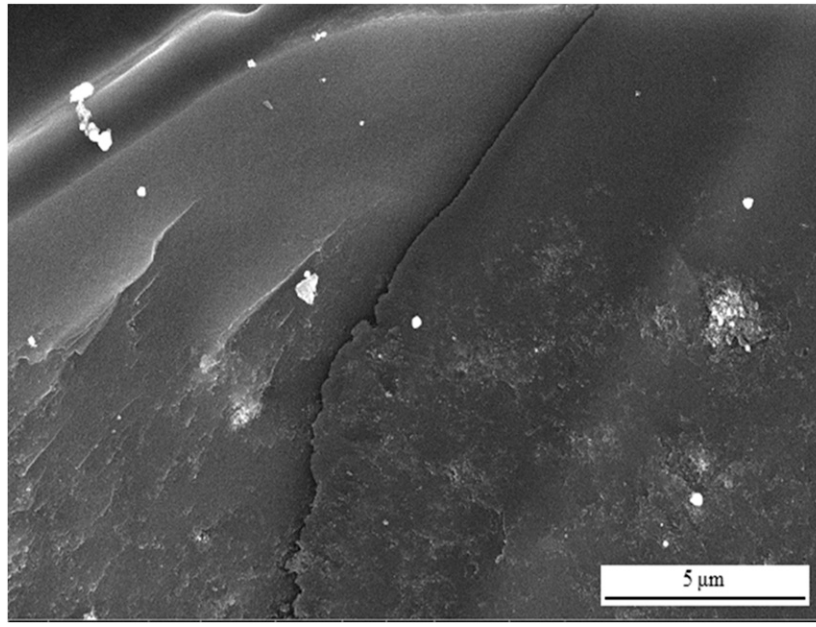

Figure 6. Scanning electron microscopy photograph of the fracture surface of nano-Fe/woodceramic composites (WCM-15).

volume electrical resistivity of the nano-Fe/woodceramic composites reduces.

Microwave Absorbing Properties

Figure 8 shows complex permittivity of the nano-Fe/woodceramic composites as a function of frequency. Generally, the real part of permittivity (ε') is related to energy storage, whereas the imaginary part of permittivity (ε'') is related to energy loss. In other words, ε' is an expression of polarization ability which arises from dipolar polarization and interfacial polarization. In this study, interfacial polarization dominates. There exist several kinds of interfaces, including the interface between α-Fe and amorphous carbon, α-Fe and glassy carbon, Fe_3C and amorphous carbon, Fe_3C and glassy carbon, and amorphous carbon and glassy carbon. ε' fluctuates with the frequency in the whole range with a decreasing trend, as shown in Fig 8a. For WCM-3 and WCM-7, there exists a distinct broad peak around 8.0 GHz arising from interfacial polarization. As the addition content of γ-Fe_2O_3 increases, the value of ε' increases at first because of the increasing of dipoles and interfaces, and the value of permittivity decreases then with the increasing of addition content of γ-Fe_2O_3. That may be because of the fact that most α-Fe and Fe_3C nanoparticles are tiny (<100 nm) and distribute uniformly in the woodceramic when the addition content of γ-Fe_2O_3 nanoparticles is relatively

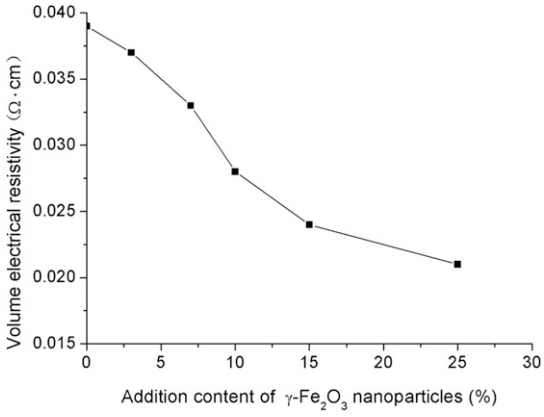

Figure 7. Influence of addition content of γ-Fe_2O_3 nanoparticles on the volume electrical resistivity of the nano-Fe/woodceramic composites.

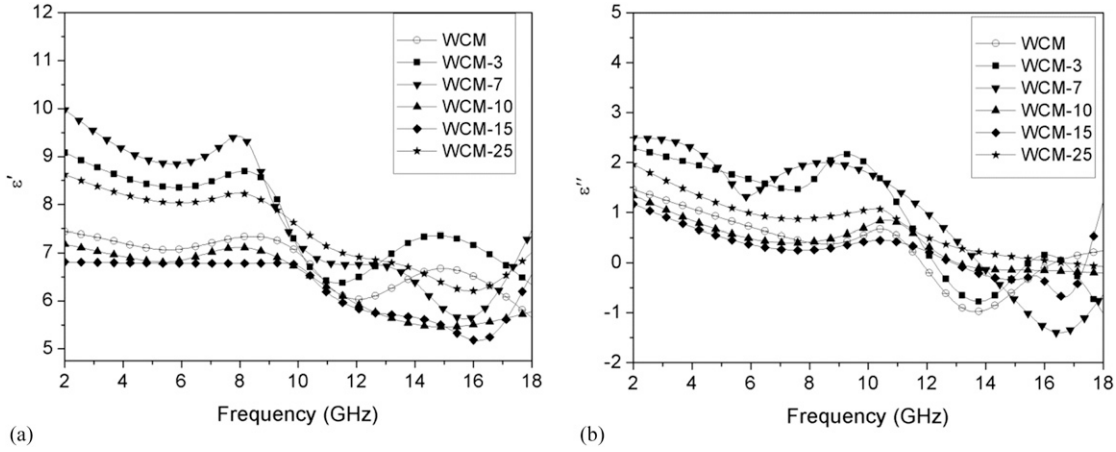

Figure 8. Complex permittivity of the nano-Fe/woodceramic composites as a function of frequency (a) real part of permittivity and (b) imaginary part of permittivity.

smaller (3% and 7%). As the addition content of γ-Fe_2O_3 nanoparticles increases (10%, 15%, and 25%), the α-Fe nanoparticles grow obviously, which leads to the reduction of the sum of interface induced by α-Fe and Fe_3C particles. As a result, interfacial polarization of the composites is weakened.

Figure 9 shows the complex permeability of the nano-Fe/woodceramic composites as a function of frequency. The real part of permeability (μ′) represents magnetization degree and the imaginary part of permeability (μ″) represents magnetic loss. μ′ of nano-Fe/woodceramic composites fluctuates in the whole range, as shown in Fig 9a. It can be seen from Fig 9b that μ″ of the woodceramics is close to 0, i.e., woodceramics nearly have no magnetic loss. μ″ of the nano-Fe/woodceramic composites first almost keeps constant around 0.05 with slight fluctuation from 2 to 14 GHz, then increases and exhibits a resonance peak at about 16 GHz and at last decreases. μ″ of WCM-7 has a strong resonance peak at about 16 Hz, whereas μ″ of WCM-10, WCM-15, and WCM-25 have weak resonance peaks at the same frequency. The peak at 16

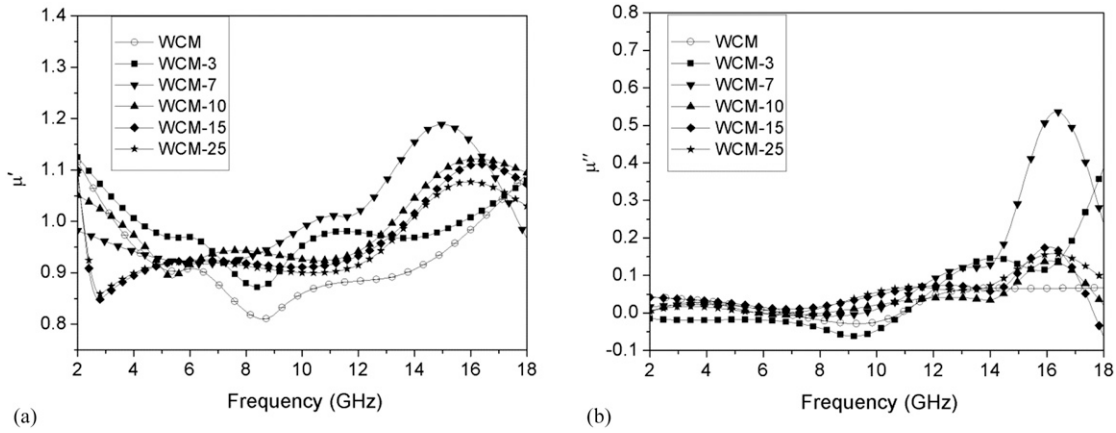

Figure 9. Complex permeability of the nano-Fe/woodceramic composites as a function of frequency (a) real part of permeability and (b) imaginary part of permeability.

GHz is related to the ferromagnetic resonance of the α-Fe nanoparticles (Liu et al 2009). Magnetic loss mainly includes eddy current loss, magnetic hysteresis loss, ferromagnetic resonance, natural resonance, and domain resonance, etc (Yamada and Otsuki 1997; Zhang et al 2006; Huo et al 2009). According to the results of volume electrical resistivity, the nano-Fe/woodceramic composites belong to semiconductor materials which can lead to eddy current loss in the dynamic magnetic field. In addition, the α-Fe nanoparticles have a higher coercivity which may lead to hysteresis loss.

Figure 10 shows the calculated RL of the nano-Fe/woodceramic composites as a function of frequency. From Fig 10, it can be observed that absorption properties of the composites are influenced by the thickness of wave-absorbed layer and addition content of γ-Fe_2O_3 nanoparticles. As the thickness of the wave-absorbed layer increases from 1 mm to 3 mm, the microwave absorption peak shifts to a lower frequency. The microwave absorption peaks of all the samples are greater than −5 dB as the thickness of wave-absorbed layer is only 1 mm. There exist two peaks as the thickness of wave-absorbed layer increases to 2 mm. The WCM-7 has the strongest absorption peak of −5.7 dB at 13 GHz.

As shown in Fig 10c, the absorption properties of the nano-Fe/woodceramic composites are improved significantly as the thickness of wave-absorbed layer increases to 3 mm. The addition content of γ-Fe_2O_3 nanoparticles has great effect on the absorption properties. The woodceramic

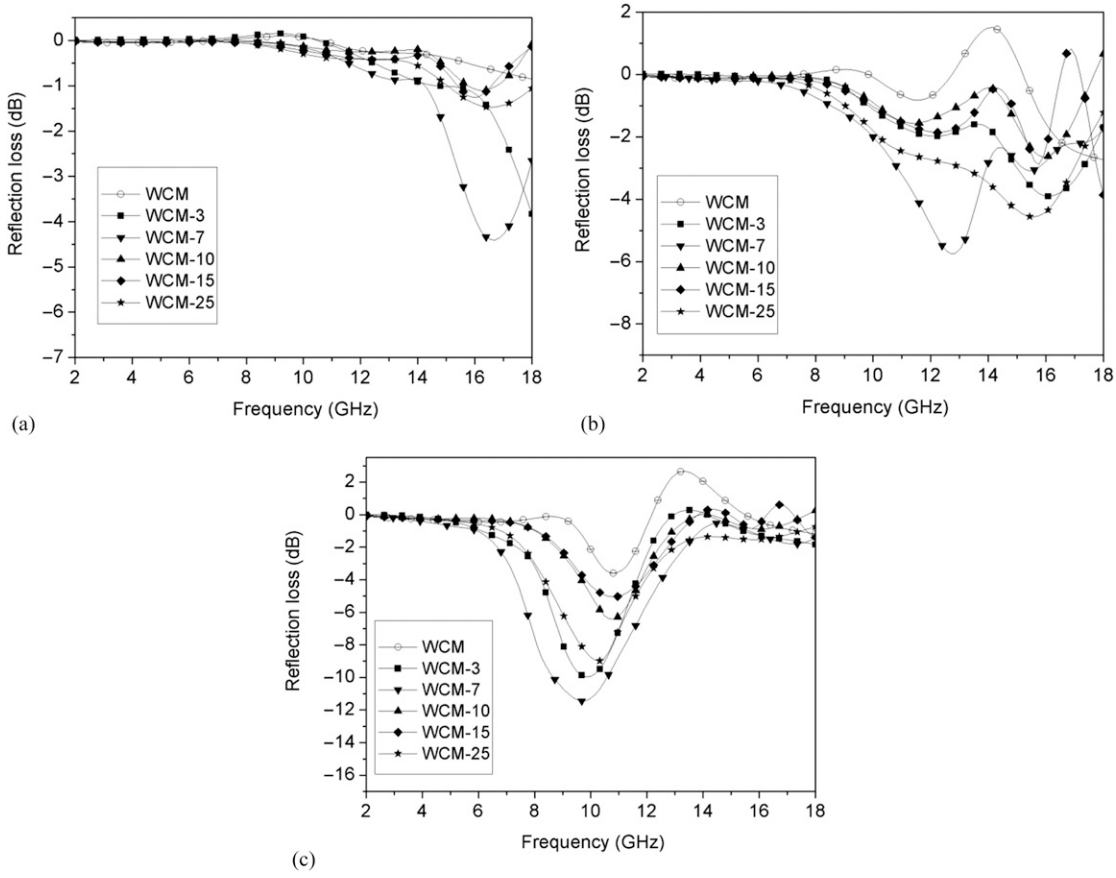

Figure 10. Reflection loss of the nano-Fe/woodceramic composites as a function of frequency (a) 1 mm (b) 2 mm (c) 3 mm.

has the worst absorption properties. The absorption properties of the nano-Fe/woodceramic composites increase at first as the addition content of γ-Fe_2O_3 nanoparticles is less than 7%, then begin to fall as the addition content of γ-Fe_2O_3 is more than 7%, and at the end increase a little as the addition content of γ-Fe_2O_3 increases from 15 to 25%. It is obvious that small and even α-Fe nanoparticles can improve the microwave absorption properties of woodceramics effectively. The minimum RL value of WCM-7 is −11.45 dB at 9.68 GHz and the corresponding frequency under −5 dB is in the range of 7.60-12.08 GHz. The minimum RL value at 3 mm is equivalent to carbon–coated nickel nanocapsules with the average size of 53 nm (Wu et al 2016) and iron-filled CNTs coated with FeCo alloy nanoparticles annealed at 450°C (Wang et al 2009). The minimum RL value of WCM-3 is −9.97 dB at 9.84 GHz and the corresponding frequency under −5 dB is in the range of 8.56-11.44 GHz. The RL value of −5 dB corresponds to 70% of EM wave attenuation. The porous structure of woodceramics make the EM waves easily irradiate and dissipate. Furthermore, the porous structure enhances the chance of multireflection which leads to the improvement of energy loss (Liu et al 2008).

CONCLUSIONS

A new kind of nano-Fe/Woodceramic composite can be fabricated from γ-Fe_2O_3 nanoparticles, Chinese fir sawdust, and furan resin. Chinese fir sawdust and furan resin change into a carbon material-woodceramic after the sintering process. α-Fe nanoparticles are in situ generated in the woodceramic during the sintering process. α-Fe nanoparticles can promote the graphitization degree of woodceramics. As a consequence, the electrical conductivity of the nano-Fe/woodceramic composites is improved compared with that of woodceramics. In addition, the mechanical properties of nano-Fe/woodceramic composites are also improved compared with those of woodceramics. The nano-Fe/woodceramic composites show good absorption properties resulting from the enhancement of interfacial polarization, ferromagnetic resonance, and multireflection owing to their porous structure. The woodceramic-based composites may become attractive candidates for the new types of EM wave absorption materials for their effective absorption performance, and electrode or motor brush for their improved mechanical and electrical conductivity performance.

ACKNOWLEDGMENTS

We are grateful for the support of the Scientific Research Fund of Hunan Provincial Education Department of China (No. 17C1662), and Youth Scientific Research Foundation of Central South University of Forestry and Technology of China (No. QJ2012012A), and the Research Foundation for Advanced Talents of Central South University of Forestry and Technology (No. 2017YJ018).

REFERENCES

Akagaki T, Hokkirigawa K, Okabe T, Saito K (1999) Friction and wear of woodceramics under oil and water lubricated sliding contacts. J Porous Mater 6:197-204.

Hirose T, Fan TX, Okabe T, Yoshimura M (2001) Effect of carbonization temperature on the basic properties of woodceramics impregnated with liquefied wood. J Mater Sci 36:4145-4149.

Hirose T, Fujino T, Fan TX, Endo H, Okabe T, Yoshimura M (2002) Effect of carbonization temperature on the structural changes of woodceramics impregnated with liquefiedwood. Carbon 40:761-765.

Hirose II, Fushitani M, Okabe T, Saito K (1999) Mechanical properties of woodceramics: A porous carbon material. J Porous Mater 6:175-184.

Huo J, Wang L, Yu HJ (2009) Polymeric nanocomposites for electromagnetic wave absorption. J Mater Sci 44: 3917-3927.

Kano M, Momota M, Okabe T, Saito K (1997) Specific heat capacity of new porous carbon materials. Woodceramics. Thermochim Acta 292:175-177.

Li J, Li SJ (2006) Pyrolysis of medium density fiber board impregnated with phenol formaldehyde resin. J Wood Sci 52:331-336.

Li SJ, Li J, Liu YX (2002) The making of woodceramics (I): From solid wood. Dongbei Linye Daxue Xuebao 30(4):5-7 [In Chinese with summary in English].

Liu QL, Zhang D, Fan TX (2008) Electromagnetic wave absorption properties of porous carbon/Co nanocomposites. Appl Phys Lett 93(1):013110.

Liu XG, Li B, Geng DY, Cui WB, Yang F, Xie ZG, Kang DJ, Zhang ZD (2009) (Fe, Ni)/C nanocapsules for electromagnetic-wave-absorber in the whole Ku-band. Carbon 47:470-474.

Liu Z, Bai G, Huang Y, Ma Y, Du F, Li F (2007) Reflection and absorption contributions to the electromagnetic interference shielding of single-walled carbon nanotube/polyurethane composites. Carbon 45(4):821-827.

Lizuka H, Fushitani M, Okabe T, Saito K (1999) Mechanical properties of woodceramics: A porous carbon material. J Porous Mater 6:175-184.

Marsh H, Crawford D, Taylor DW (1983) Catalytic graphitization by iron of isotropic carbon from polyfurfuryl alcohol, 725-1090 K. A high resolution electron microscope study. Carbon 21:81-87.

Oh JH, Oh KS, Hong CS (2004) Design of radar absorbing structures using glass/epoxy composite containing carbon black in X-band frequency ranges. Compos Part B Eng 35(1):49-56.

Okabe T, Saito K, Hokkirigawa K (1996) Effect of burning temperature on the structure changes of woodceramics. J Porous Mater 2:215-221.

Qian JM, Jin ZH, Wang JP (2004) Structure and basic made from phenolic resin-basswood powder composite. Mater Sci Eng A 268:71-79.

Shibata K, Okabe T, Saito K, Okayama T, Shimada M, Yamamura A, Yamamoto R (1997) Electromagnetic shielding properties of woodceramics made from wastepaper. J Porous Mater 4:269-275.

Wang C, Lv RT, Kang FY, Gu JL, Gui XC, Wu DH (2009) Synthesis and application of iron-filled carbon nanotubes coated with FeCo alloy nanoparticles. J Magn Magn Mater 321:1924-1927.

Wu WT (2008) Preparation and properties of carbon composite from bagasse/wheat straw with different adhensives. Nongye Gongcheng Xuebao (Beijing) 24:204-207 [In Chinese with summary in English].

Wu ND, Liu XG, Zhao CY, Cui CY, Xia AIL (2016) Effects of particle size on the magnetic and microwave absorption properties of carbon-coated nickel nanocapsules. J Alloys Compd 656:628-634.

Xing SL, Yang YF, Wu YQ (2010) Research on biological ceramics produced by cotton stalks. Mater Rev 24: 114-116 [In Chinese with summary in English].

Xu YG, Zhang DY, Cai J, Yuan LM, Zhang WQ (2013) Microwave absorbing property of silicone rubber composites with added carbonyl iron particles and graphite platelet. J Magn Magn Mater 327:82-86.

Yamada S, Otsuki E (1997) Analysis of eddy current loss in Mn-Zn ferrites for power supplies. J Appl Phys 81:4791-4793.

Yu XC, Sun DL, Sun DB, Xu ZH, Li XS (2012) Basic properties of woodceramics made from bamboo powder and epoxy resin. Wood Sci Technol 46:23-31.

Zhang XF, Dong XL, Huang H, Liu YY, Wang WN, Zhu XG, Lv B, Lei JP (2006) Microwave absorption properties of the carbon-coated nickel nanocapsules. J Appl Phys 89:053115.

Zhang D, Xie XQ, Fan TX (2005) Morphology and damping characteristics of woodceramics. J Mater Sci 37:4457-4463.

Zhao BY, Hirose T, Okabe T, Zhang D, Fan TX, Hu KA (2002) Woodceramics Prepared from wood powder/phenolated wood composite. J Porous Mater 9:195-201.